Structure and Properties of Alkylammonium Monolayers Self-Assembled on Montmorillonite Platelets

Maged A. Osman,*,† Michael Ploetze,‡ and Peter Skrabal§

Institute of Polymers, D-MATL, ETH, CH-8092 Zurich, Switzerland, Laboratory of Clay Mineralogy, IGT, D-BAUG, ETH, CH-8093 Zurich, Switzerland, and Institute for Chemical and Bioengineering, D-CHAB, ETH, CH-8093 Zurich, Switzerland

Received: September 8, 2003; In Final Form: December 7, 2003

Monolayers of mono-, di-, tri-, and tetraalkylammonium cations of varying chain length (C_4, C_8, and C_{18}) were self-assembled on montmorillonite platelets. The structure and chain dynamics of these SAMs were probed by infrared spectroscopy (IR), nuclear magnetic resonance spectroscopy (NMR), X-ray diffraction (XRD), and differential scanning calorimetry (DSC). Depending on the cross-sectional area, the available area/cation, and the alkyl chain length, the molecules adopt a two-dimensional order or a disordered state at ambient temperatures. Short alkyl chains lie flat, disordered on the substrate surface as long as there is enough space. With increasing volume of the organic layer between two silicate layers facing each other, the chains force the layers to enlarge their basal-plane spacing but remain disordered. At a certain length and number of chains, the molecules adopt an ordered state due to increasing chain interactions and packing density. To minimize their conformational entropy and maximize their packing density, the chains attached to platelets facing each other interdigitate. The average molecular axis in the organic thin film is inclined to the montmorillonite surface normal by an angle, which depends on the packing environment and the geometry of the molecules. In the ordered state, the alkyl chains preferentially assume an all-trans conformation. With increasing temperature, conformational transformation of the chains takes place, leading to a dynamically disordered phase (liquidlike). Although the translational freedom of the chains is restricted by the electrostatic binding of the headgroups to the substrate, the conformational transformation leads to chains with random conformation and destroys the two-dimensional order. The phase transition manifests itself in an increase in basal-plane spacing as well as in IR absorption frequency and carbon resonance shifts accompanied by an entropy change. The density of the organic ultrathin film confined between two silicate layers seems to decrease on heating across the phase transition, leading to an increase in volume and consequently in the organic layer thickness and in *d*-spacing, respectively. The basal-plane spacing of 3C18 and 4C18 is appreciably larger than that of C18 and 2C18, which is advantageous for exfoliation in the synthesis of polymer nanocomposites.

Introduction

Montmorillonite is an expandable dioctahedral smectite with a mean layer charge of 0.2−0.5 equiv/mol and belongs to the family of the 2:1 phyllosilicates.[1,2] Its particles consist of stacks of aluminosilicate 2:1 layers with a regular gap between (interlayer). These layers are ∼0.95 nm thick and comprise two modular units: tetrahedral and octahedral sheets. A tetrahedral sheet is composed of corner-linked tetrahedra, whose central ions are Si^{4+} or Al^{3+} and sometimes Fe^{3+}. The basal oxygens of a tetrahedron are shared by the neighboring tetrahedra, forming a hexagonal pattern. For a given tetrahedral sheet, all apical oxygens point in one direction and at the same time form a part of the adjacent octahedral sheet. The octahedral sheet is composed of edge-shared octahedra with Al^{3+}, Mg^{2+}, Fe^{3+}, or Fe^{2+} typically serving as the coordinating cation. Due to isomorphic substitutions in the lattice, the layers have a permanent negative charge. The most common substitution is Mg^{2+} for Al^{3+} in the octahedral sheet. Neutrality on the surface and in the interlayer is restored by cations or hydrated cations. The electrostatic forces holding the layers together are relatively weak, and the interlayer distance varies depending on the radius of the cation present and its degree of hydration. As a result, the stacks swell in water and the layers can be easily exfoliated on shearing.

Industrially, montmorillonite has been exploited in different applications varying from thixotropic agents in paints and cosmetics to adsorbents in treatment of contaminated waste streams and fillers in polymer nanocomposites.[3−5] In most of these applications, it is necessary to exchange the inorganic cations present by organic ions compatible with the matrixes, in which the mineral is going to be embedded. Alkylammonium ions of different chain lengths have been often used to build an ionically bonded thin organic film on the surface of the montmorillonite layers. The structure and properties of these ultrathin films are important for the final properties of the heterogeneous material because they influence the particle−particle and particle−matrix interactions. Phase separation or depletion may result from entropic or enthalpic differences at the interface. Traditionally, structural characterization of these films has been limited to X-ray diffraction analysis. On the basis of basal-plane spacing measurements, Weiss[6] suggested that the

* Corresponding author. Phone: +41 1 632 46 53. Fax: +41 1 632 10 96. E-mail: mosman@mat.ethz.ch.
† Institute of Polymers.
‡ Laboratory of Clay Mineralogy.
§ Institute for Chemical and Bioengineering.

10.1021/jp0366769 CCC: $27.50
Published on Web 01/22/2004

alkyl chains might lie flat or assume a tilted upright position to the aluminosilicate surface depending on the charge density of the substrate and the length of the chains. Lagaly et al.[3,7−9] postulated that the alkyl chains lie flat on the silicate surface in "monolayer, bilayer, pseudotrimolecular arrangement" (through kink formation) or radiate away from the surface "paraffin-type", depending on the charge density and the chain length.

Vaia et al.[10] studied the structure of dioctadecyldimethylammonium films on montmorillonite with varying mean charge density by X-ray diffraction (XRD), infrared spectroscopy (IR), and differential scanning calorimetry (DSC) and showed that the alkyl chains assume an ordered state. That is, the alkylammonium cations build a self-assembled monolayer (SAM) on the mineral surface. The authors postulated molecular arrangements varying from solidlike to liquidlike and in intermediate cases liquid crystalline, depending on the packing density and chain length. However, it is not clear how a monolayer of tethered alkyl chains can adopt a liquid crystalline order, neither nematic nor smectic. No liquid crystalline phase has been yet reported in alkanes of similar chain lengths, presumably due to the relatively small energy differences between the trans and gauche conformers in these chains. Besides, different clays with varying mean charge densities were used as substrates to elucidate the influence of the packing density on the structure of the organic film. It is well-known that the charge distribution in smectites is heterogeneous and the inhomogeneity differs from one clay to the other; i.e., the distribution and consequently the packing density of the alkyl chains assembled on different clay surfaces is expected to differ.[3,9,11]

The goal of the present study was to investigate the structure and properties of alkylammonium monolayers self-assembled on a montmorillonite surface as well as their dependence on the chain length and packing density. For this purpose, mono-, di-, tri-, and tetraalkylammonium ions of varying chain length (butyl, octyl, and octadecyl) were assembled on one single Wyoming montmorillonite. The phase behavior and chain dynamics of the resulting monolayers were investigated by IR, XRD, DSC, and nuclear magnetic resonance spectroscopy (NMR).

Experimental Section

Materials. The ammonium salts were purchased from Fluka, Buchs, Switzerland, and were used without further purification. Millipore Ultrapure water (pH = 5.8, G = 1 μS/cm) was employed in all experiments. Wyoming montmorillonite (volclay) was obtained from C. G. Meier-Gaissert (Zurich, Switzerland). Volclay is a natural Na bentonite, which has a mean layer charge of 0.28 equiv/mol (determined by the alkylammonium method),[3,9,12] and a cation exchange capacity (CEC) of 0.72 mequiv/g. The CEC was determined by exchanging the Na^+ ions with $Cu(trien)^{2+}$ and measuring the decrease in its concentration photometrically.[13,14] For this purpose, 50 g of 5 mM $CuSO_4$ solution was mixed with 52.5 g of 5 mM triethylenetetramine solution to give the $Cu(trien)^{2+}$ solution, whose exact molality was calculated. The extinction coefficient ($\approx$4.85) of this standard solution at λ_{255} was measured on a Cary 1E spectrometer (Varian, Palo Alto, CA). A 20−30 mg sample of the clay was dispersed (shaking and sonication with an ultrasonic horn at 60% amplitude for 5 min) in 15 g of water in a polypropylene (PP) vial, and then 12 g of the $Cu(trien)^{2+}$ solution was added and the mixture shaken for 30 min. The suspension was then centrifuged and the supernatant liquid filtered through a cellulose acetate filter with 0.45 μm pore diameter (Schleicher and Schuell, Dassel, Germany). The first 2 mL of the filtrate was discarded to avoid contamination and adsorption by the filter. The concentration of $Cu(trien)^{2+}$ in the filtrate was measured and the amount of exchanged ions calculated. The CEC was calculated by taking the valency of the $Cu(trien)^{2+}$ into consideration.

Exchange Reaction. A 2 g sample of the mineral was dispersed in a mixture of 100 mL of water and 60 mL of ethanol by stirring at 70 °C for 1 h and sonication (ultrasonic horn at 60% amplitude) for 10 min. To this dispersion was added dropwise under stirring the required amount of ammonium salt, dissolved in 40 mL of ethanol, and the reaction mixture was stirred at 70 °C for 48 h. At the end of the reaction time, the suspension was filtered and the organosilicate thoroughly washed with a hot ethanol−water mixture (1:1) followed by hot ethanol. The product was suspended (sonicated) and stirred in hot ethanol for 3 h, filtered, and dried at 70 °C under reduced pressure. This process was repeated if the TGA showed the presence of unreacted ammonium salt or local bilayer.[15] For the preparation of all butyl (C4−4C4) and octyl (C8−4C8) montmorillonite, an excess (150% of the CEC) of the ammonium salts was used, and the exchange reaction was repeated to ensure complete exchange of the sodium ions. These precautions were not necessary in the case of the octadecyl derivatives (C18−4C18) due to the high affinity of these ammonium ions to the mineral, and an amount of salt equivalent to 100% of the CEC was used. The reaction time was also reduced to 24 h.

Due to the low solubility of the trioctadecylmethyl and tetraoctadecylammonium bromides, the 3C18 and 4C18 were prepared as follows: 2 g of the mineral was dispersed in a mixture of 100 mL of water and 150 mL of ethanol by stirring at 70 °C for 1 h and sonication (ultrasonic horn at 60% amplitude) for 10 min. To this dispersion was added portionwise under stirring the required amount of solid ammonium salt (corresponding to 100% of the CEC). Each portion was one-fifth of the total amount of salt, and the portions were added in 1 h intervals. The reaction mixture was stirred for further 24 h at 70 °C. At the end of the reaction time, the suspension was left shortly to settle and the supernatant liquid decanted. Fresh ethanol was added and the suspension stirred at 70 °C for 1 h before the alcohol was decanted again. This procedure was repeated twice before the product was filtered and washed with hot ethanol. The product was suspended (sonicated) and stirred in an ethyl acetate−ethanol mixture 4:1 for 3 h, then filtered, and dried at 70,°C under reduced pressure. The presence of local bilayer or unreacted ammonium salt as well as the completeness of the exchange was controlled by thermogravimetric analysis.[15]

Thermal Analysis. High-resolution (Hi-Res) thermogravimetric analysis (TGA), in which the heating rate is coupled to the mass loss, that is, the sample temperature is not raised until the mass loss at a particular temperature is completed, was performed on a Q500 thermogravimetric analyzer (TA Instruments, New Castle, DE). All measurements were carried out in an air stream under the same conditions. The mass loss with increasing temperature as well as its first derivative (DTG) that represents the change in decomposition rate were plotted.

The differential scanning calorimetry (DSC) was carried out under nitrogen at a heating or cooling rate of 10 °C/min on a DSC 7 (Perkin-Elmer, Norwalk, CT). Two heating and one cooling run were consecutively carried out in a cycle and the peak maxima were considered as the transition temperatures.

IR Spectroscopy. Infrared transmission spectra were collected on a Bruker IFS 66V FTIR spectrometer (Bruker Optics Inc, Billerica, MA) equipped with a liquid nitrogen cooled MCT

(Hg−Cd−Te) detector, operating at a resolution of 0.5 cm^{-1} with an unpolarized beam striking the powder sample held between CaF_2 windows at normal incidence. A temperature-controlled cell and a Fenwal controller Series 550 were used to thermostat the sample (Fenwal Inc., Ashland, MA). The cell was gradually heated to the desired temperature and maintained there for at least 5 min before the spectrum was acquired. The temperature of the cell body was registered by an additional thermocouple. The peak maximum was considered as the line position.

NMR Spectroscopy. Proton decoupled solid state ^{13}C NMR spectra (100.65 MHz) were recorded by one-pulse excitation of the carbons with a pulse-repetition delay of 5 s to ensure comparable signal intensities for the different resonances. All spectra were recorded on a Bruker AVANCE 400 MHz spectrometer equipped with a standard 4 mm variable-temperature double-resonance magic-angle spinning (MAS) probe. A comparison of preliminary spectra, obtained at spinning rates of 10 and 14 kHz, showed that no further reduction of the line width at 14 kHz could be achieved. Therefore, a spinning rate of 10 kHz was used, accumulating 512−16k scans, as indicated in the figure legends. To avoid any truncation of the free induction decays (FIDs) at high temperatures (longer FIDs), always 2048 (2k) data points/scan have been used. The $\pi/2$ pulse length on the carbon channel was 3.5 μs, and heteronuclear spin decoupling was achieved by two-pulse phase modulation (TPPM) with a pulse length of 4.6 μs and a phase angle of 20°.[16]

The temperature was calibrated using the temperature dependence of the ^{13}C chemical shifts of samarium acetate, as well as the ^1H shift differences of methanol signals on tetrakis(trimethylsilyl)silane.[17−19] The accuracy of the temperature calibration is estimated to be ca. ±5 °C with a temperature gradient of about 5 °C over the length of the rotor.[20,21] The FIDs were processed by zero filling the first 512 or 1k complex data points (see figure legends) to 16k data points (8k in the real part of the spectrum with a width of 35 211 Hz) for a resolution of 4.3 Hz/point. Window functions were applied as indicated in the figure legends. The chemical shifts are referenced to external TMS.

X-ray Diffraction. Wide-angle X-ray diffraction patterns (WAXRD) were collected at room temperature in Bragg−Brentano geometry with a $\Theta - \Theta$ diffractometer (D8 Advance, Bruker AXS) using Cu Kα radiation (λ = 0.154 18 nm). The instrument was equipped with an automatic divergence and antiscattering slit, a graphite monochromator and a NaI scintillation counter. The powder samples were step-scanned at room temperature from 1.5 to 65° 2Θ (step width 0.02° 2Θ, counting time 3 s). Temperature dependent diffractograms were obtained by mounting the powder samples in a sample chamber (TTK 450, Anton Paar) with controlled temperature and humidity. The relative humidity (RH) in the chamber was adjusted by mixing wet and dry pressurized air with a humidity controller (Sycos H). The RH in the chamber was stabilized at 2% (±0.2%) for 2 h before starting the measurements. The samples were thermostated at each temperature for 3 min before they were step-scanned from 1.5 to 45° 2Θ. To enhance the basal reflections of the clay mineral, a preferred orientation of the platelets was induced by pressing and smearing the sample surface in the holder with a glass slide. The (001) basal reflection of an internal standard muscovite (2Θ = 8.84°) was used to calibrate the line position of the organo-silicate reflections. To determine the peak positions, the diffractograms were fitted with a split Pearson VII function (TOPAS P profile fitting program, Bruker AXS) and the basal-plane spacing (d_{001}) was calculated applying Bragg's law.

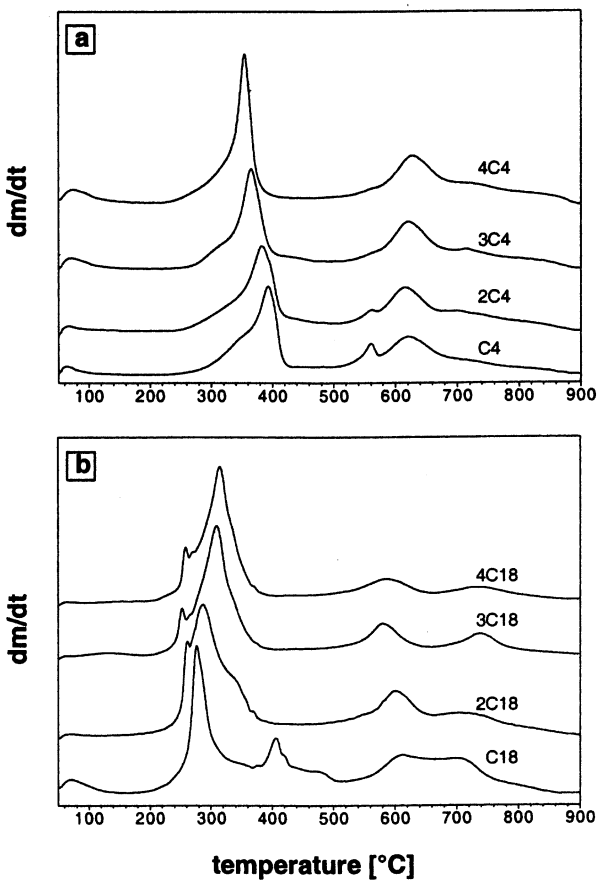

Figure 1. Differential thermogravimetric (DTG) plots of (a) C4−4C4 and (b) C18−4C18.

Results

To investigate the structure and properties of monolayers self-assembled on montmorillonite, it is necessary to ensure that the cation exchange is complete and that only ionically bonded molecules are present. This was monitored by TGA, which proved to be a suitable method for detecting both bonded and nonbonded organic molecules.[15,22−24] It has been shown that the presence of free ammonium salt or local bilayer molecules is indicated by additional peaks in the DTG plots at temperatures lower than that of the first decomposition event of the SAMs.

Thermal Analysis. The DTG plots of the short alkylammonium SAMs (C4−4C4 and C8−4C8) showed one decomposition event below 400 °C (e.g., Figure 1a), indicating that they are free from impurities, whereas traces of intercalated molecules (local bilayer) were still present in 2C18−4C18 (peak at ca. 260 °C in Figure 1b). These impurities were difficult to get rid of due to the low solubility of some alkylammonium salts and the dense packing of long alkyl chains. Complete exchange of the inorganic cations was ensured by achieving a mass loss in the TGA equivalent to the CEC of the clay in cases where complete oxidation of the organic matter was possible.[15] When the TGA residue was dark in color, indicating incomplete oxidation, the exchange reaction was repeated until no increase in surface coating could be detected by TGA.

The calorimetric behavior of the alkylammonium monolayers was scanned between −30 and +150 °C at a rate of 10 °C/min. All butyl (C4−4C4) and octyl (C8−4C8) derivatives showed no abrupt change in enthalpy with increasing temper-

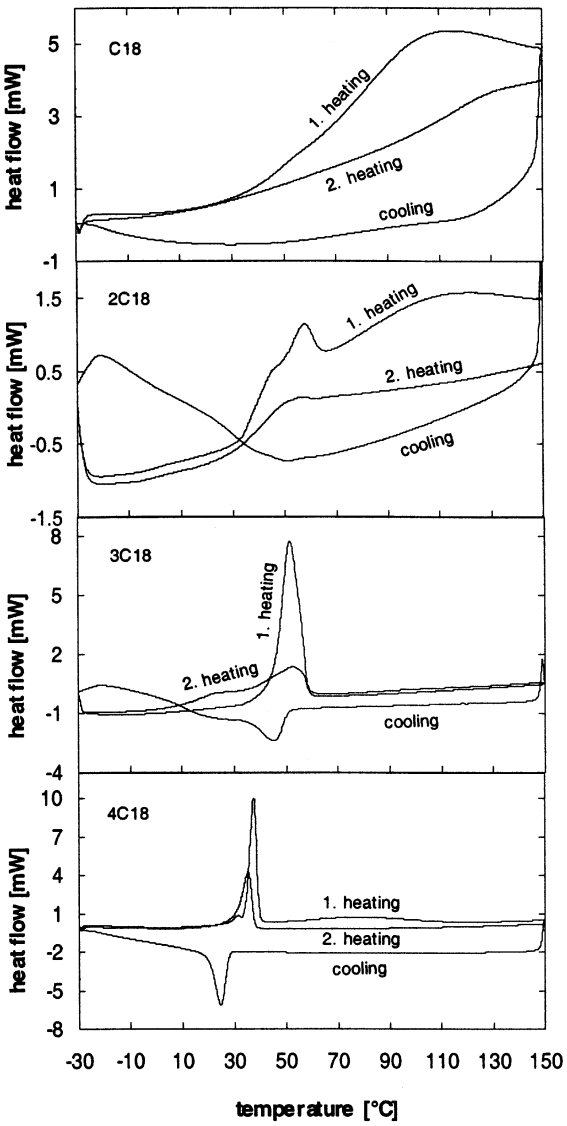

Figure 2. Differential scanning calorimetric (DSC) traces of C18−4C18.

TABLE 1: Phase Transition Temperatures and Enthalpies of Alkylammonium SAMs on Montmorillonite

organo-montmorillonite	transition temp (°C)	transition enthalpy (1. heating) [kJ/mol]
C18		
2C18	57	5.7
3C18	51	30.4
4C18	37	26.9

ature, whereas 3C18 and 4C18 showed distinct peaks (Figure 2, Table 1), indicating first-order transitions. In both cases, the transitions were reversible but the samples needed time to fully recover; that is, the maximum possible ΔH was reached after standing at room temperature (RT) for several hours. In C18, no transition was detected even after cooling at −30 °C for 1 h and an appreciable amount of moisture was adsorbed on the mineral surface, which gradually evaporated on heating, suggesting that the alkyl chains do not completely cover the surface. 2C18 showed a broad small peak at 57 °C preceded by a shoulder at ca. 40 °C, which was not completely reversible at the cooling rate used. The mineral surface was also still hygroscopic despite the organic coating, as indicated by the heat flow between 70 and 130 °C, and the weight loss below 150 °C (TGA), but the moisture was less than in C18. The transition

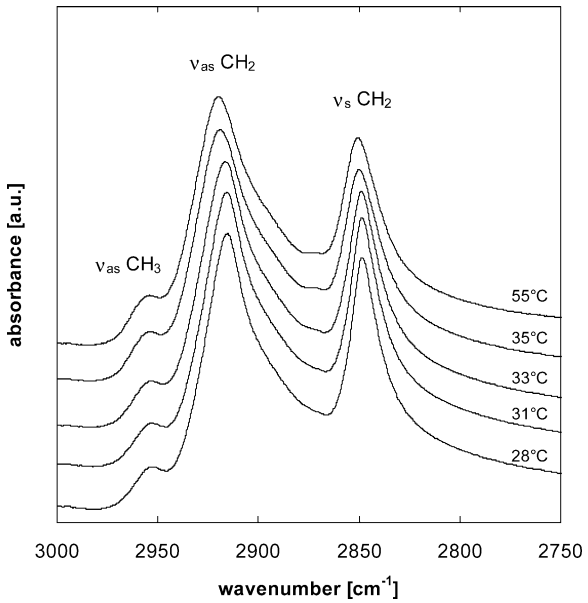

Figure 3. Transmission IR spectra of 4C18 in the C−H stretching region at different temperatures.

enthalpies of 3C18 and 4C18 were substantially (ca. 5-fold) higher than that of 2C18, and the mineral surface was hydrophobic (Figure 2, Table 1). The peak full width at half-height (fwhh) also decreased with increasing number of *N*-alkyl chains and a relatively sharp peak was observed for 4C18. However, if the onset of the heat flow is considered, it can be seen that the transformation extends over a temperature range of ca. 20−30 °C. On cooling, the peaks were generally broader, and an increased tendency to supercool was observed with decreasing number of chains.

Infrared Spectroscopy. In agreement with the DSC measurements, the $\nu_{as} + \nu_s$ CH_2 absorption bands of C4−4C4 and C8−4C8 did not show any temperature dependence. The frequency of the methylene stretching bands of C18 also showed no shift up to 70 °C. In contrast, the methylene absorption bands of 3C18 and 4C18 were shifted to higher frequencies with increasing temperature. Figure 3 shows the high-frequency region of the absorption spectra of 4C18 in the temperature range 28−55 °C. The temperature dependence of $\nu_{as}(CH_2)$ and $\nu_s(CH_2)$ (peak maxima) for 3C18 and 4C18 is plotted in Figure 4, showing distinct shifts to higher wavenumbers (ν_{as} ca. 5 cm^{-1} and ν_s ca. 2.5 cm^{-1}) at approximately the same transition temperatures measured by DSC. The temperatures indicated by the DSC peak maxima corresponded to those at which most of the frequency shift was accomplished. It may be remarked that the transition temperatures given in Table 1 are peak maxima but the transitions take place over a temperature range as seen in the DSC traces (Figure 2). The asymmetric CH_2 stretching band of 2C18 showed a similar increase in wavenumber with temperature (Figure 4) but the shift was smaller (ca. 1.5 cm^{-1}). In 2C18, the accuracy of line position determination of $\nu_s(CH_2)$ did not allow the detection of the wavenumber shift with temperature (a shift smaller than 1 cm^{-1} is expected).

NMR Spectroscopy. The ^{13}C spectra of the organically modified volclay give insight into the dynamic behavior of the octadecyl chains as a function of their number and temperature. Figure 5 shows a comparison between the NMR spectra of 2C18 mica (sample from ref 24) and those of 4C18 volclay in the temperature range −19 to +65 °C. The assignment of the ^{13}C resonances for the volclay SAM is in agreement with that reported for 2C18 mica.[24] The temperature dependence is also

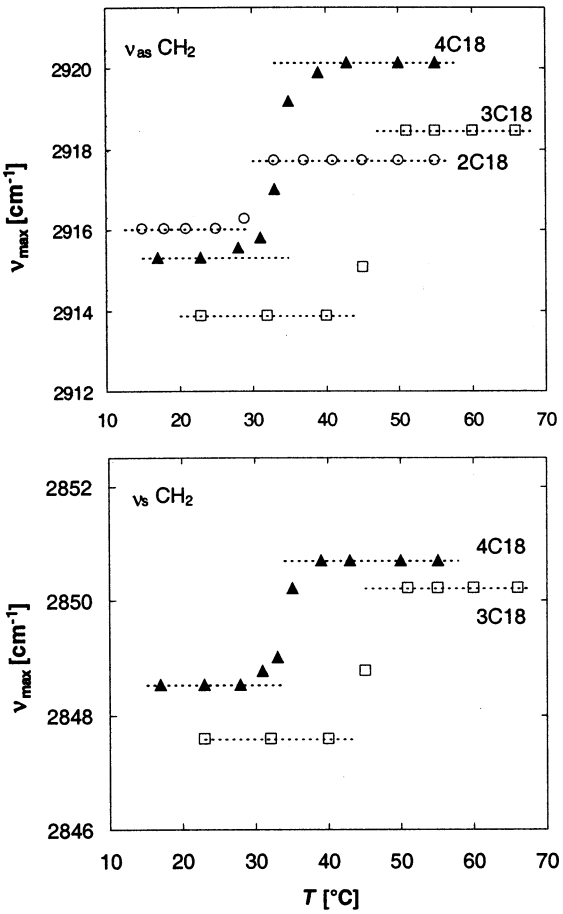

Figure 4. Temperature dependence of the methylene C−H symmetric and asymmetric stretching vibration frequencies (peak max.) of 2C18−4C18. The dotted lines are simply a guide for the eye.

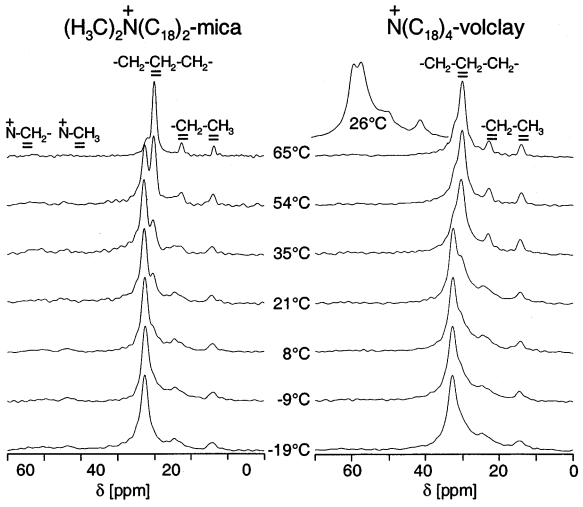

Figure 5. Temperature dependence and assignment of ^{13}C resonances of 2C18 mica and 4C18 volclay. 2C18 mica: 618, 800, 800, 757, 2k, 2k, 2k scans accumulated with decreasing temperature. 4C18 volclay: 512 scans each. A total of 700 (2C18 mica) and 512 (4C18 volclay) data points of the FIDs used for processing, line broadening 10 Hz. Inset: 8k scans accumulated at 26 °C; 512 data points of the FID used, 10 Hz line broadening.

quite similar. At −19 °C, the all-trans conformation of the methylene groups (C2−C16) dominates, giving a line at 32.5 ppm for 2C18 mica and 32.8 ppm for 4C18 volclay. With increasing temperature the mobility of the chains increases and the all-trans conformation gradually changes to a dynamic average of the trans and gauche conformers, leading to narrower

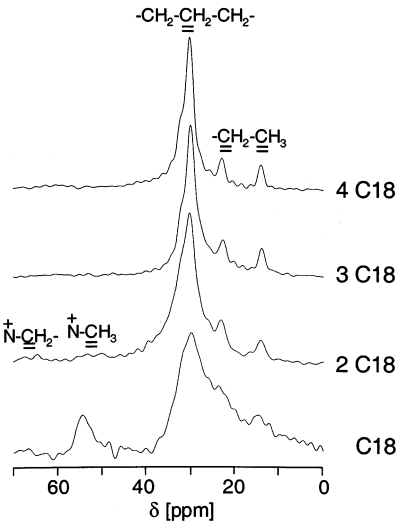

Figure 6. ^{13}C spectra of C18−4C18 volclay at 65 °C. 2k, 1k, 1k, and 512 scans accumulated (from C18 to 4C18); 512 data points of the FIDs used, line broadening 10 Hz.

resonances with chemical shifts of 29.8 and 30.1 ppm for mica and volclay, respectively. In contrast to 2C18 mica, the two magnetic sites of 4C18 volclay are only resolved at 26 °C (inset in Figure 5), at which temperature the ratio of the two sites is ca. 1:1, because of its broader lines. The line widths of 4C18 volclay are larger than those of 2C18 mica (ca. 260 Hz and ca. 150 Hz at 65 °C, respectively) probably due to looser packing and more heterogeneous cation distribution on the montmorillonite surface. Nevertheless, the shoulder of the second magnetic site is clearly observed on either side of the dominating resonance, depending on temperature. The CH_3 and CH_2 groups directly attached to the N atom (expected at ca. 53 and 63 ppm, respectively) are very broad and hard to detect. Besides, the residual dipolar coupling to the ^{14}N nuclei (not averaged away by MAS) may contribute to this broadening by a reduced mobility of the headgroups compared to the carbon atoms further away along the chains.

The spectra of C18−4C18 volclay at 65 °C are compared in Figure 6, showing that the line width increases with decreasing number of chains and that the dynamic average of the trans/gauche conformers dominates at this temperature. The chemical shifts (in the order 4C18 to C18) are C2−C16 at 30.1, 29.9, 30.1, and 29.8 ppm; C17 at 22.9, 22.7, 23.1, and ca. 23.7 ppm; C18 at 14.1, 13.9, 14.1, and ca. 14.6 ppm; N−CH_3 of C18 volclay at ca. 54 ppm. The temperature dependence of the ^{13}C spectra (10−45 ppm) of 2C18−4C18 volclay is shown in Figure 7. As can be seen, the two magnetic sites of the CH_2 groups in 3C18 are partially resolved at 35 °C, comparable to those of 4C18 at 26 °C (inset in Figure 5), because the conformers' ratio is close to 1:1. The chemical shift changes from 32.7 ppm at −19 °C (all-trans) to 29.9 ppm at 65 °C (averaged trans/gauche). The inhomogeneous line broadening of 2C18 is larger than that of 3C18 or 4 C18 and the transition from dynamically averaged trans/gauche CH_2 conformation to dominating all-trans could not be observed in the investigated temperature range. At −19 °C, the ratio of all-trans to averaged trans/gauche conformers is close to 1:1 and shifts slowly over a broad temperature range to a dominating dynamic average. This is confirmed by the two insets in Figure 7, which show spectra of 12k accumulated scans at 2 and 35 °C, resolution enhanced by the application of Lorentz−Gauss window functions with −250 Hz line broadening (LB) and Gauss broadening (GB) of 0.45 to the FIDs (1k data points used). Because the ^{13}C spectra of C18 did not show

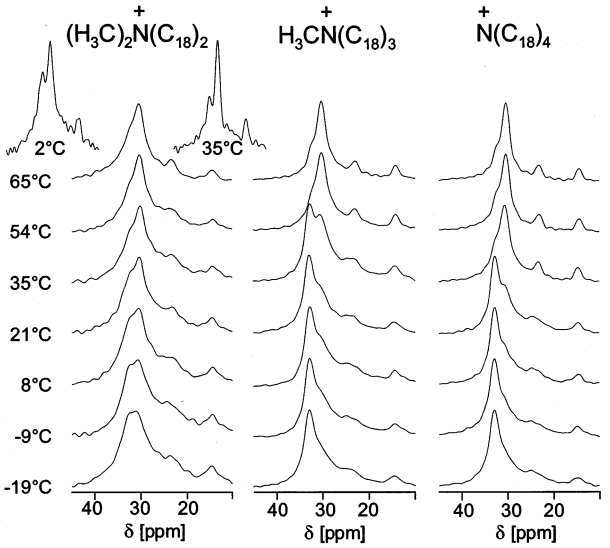

Figure 7. Temperature dependence of the ^{13}C resonances (C2−C16) of 2C18−4C18 volclay. 512, 1k, and 1k scans accumulated (from 4C18 to 2C18). Insets of 2C18: for resolution enhancement at 2 and 35 °C, 12k scans were accumulated and the first 1k data points of the FIDs were zero filled to 16k. The resolution was enhanced with a Lorentz−Gauss window function (line broadening LB = −250 Hz).

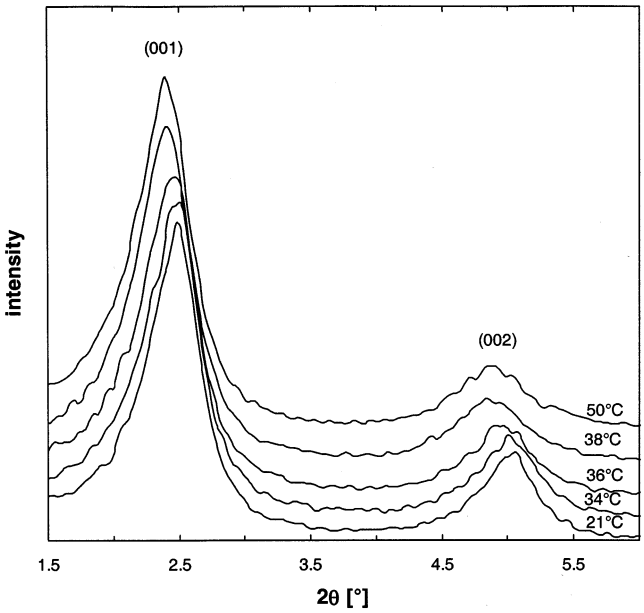

Figure 8. Wide-angle X-ray diffraction (WAXRD) patterns of 4C18 at different temperatures.

any temperature dependence, the spectra were not shown in Figure 7. However, this observation is in agreement with the fact that no transition was observed in DSC (Figure 2).

X-ray Diffraction. Temperature dependent measurements of the (001) basal-plane reflection of 4C4, 4C8, and C18 showed that the change in their basal-plane spacing (*d*-spacing) up to 70 °C is within the accuracy of the measurement. In contrast, the d_{001} of 2C18−4C18 increased at temperatures corresponding to the transition temperatures observed in DSC, IR, and NMR spectra. To illustrate the dependence of the basal reflections on temperature, the diffractograms of 4C18 recorded in the temperature range 21−50 °C are stacked in Figure 8. The temperature dependence of the d_{001} of 2C18−4C18 is plotted in Figure 9, showing that the increase in *d*-spacing of 4C18 is 0.14 nm, whereas that of 3C18 is 0.04 nm and that of 2C18 is 0.02 nm. It may be remarked that the DSC peak temperatures

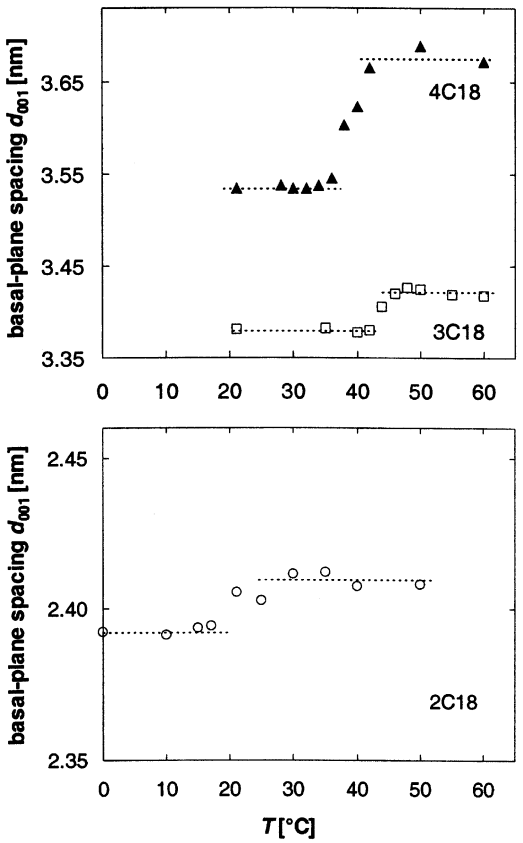

Figure 9. Temperature dependence of the basal-plane spacing of 2C18−4C18. The dotted lines are simply a guide for the eye.

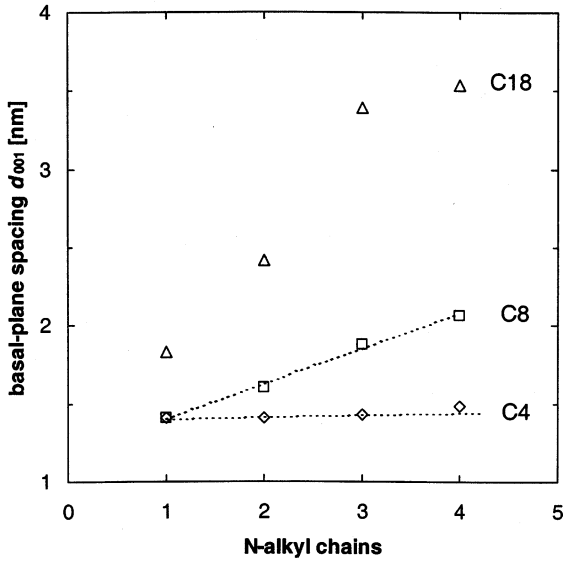

Figure 10. Dependence of the basal-plane spacing on the number of alkyl chains, of different length, in the organic cation at room temperature. The dotted lines are simply a guide for the eye.

correspond to those at which most of the basal-plane spacing increase was achieved. Because the dimensions of the aluminosilicate layers remain constant in this temperature range, the increase in *d*-spacing actually reflects the change in the organic film thickness with temperature. The increase in *d*-spacing with growing number of alkyl chains attached to the nitrogen atom at room temperature is shown in Figure 10. At a chain length of four carbon atoms (C4), there was no change in the basal-plane spacing up to three chains, then a slight increase (0.05 nm) was observed on increasing the number of chains to four

(4C4). In the octyl series (C8−4C8), the *d*-spacing increased linearly with growing number of chains and the increment was ~0.2 nm/chain. In the octadecyl series (C18−4C18), the increase in d_{001} was nonlinear. Up to 3C18 the increase per chain was appreciable but there was only a small difference in spacing between 3C18 and 4C18. The *d*-spacing of 3C18 and 4C18 at RT was 3.38 and 3.54 nm, respectively, which is appreciably larger than that of C18 and 2C18 (1.83 and 2.39 nm, respectively). This is advantageous for exfoliation in the synthesis of polymer nanocomposites.

Discussion

The molecules of long mono- and dialkylammonium SAMs assembled on mica have been shown to assume tilted vertical positions on the substrate surface.[22,24] In contrast to muscovite mica, where the net layer charge is defined (1.0) and the surface area per cation is 0.47 nm^2, the mean layer charge density of montmorillonite varies from one clay to the other between 0.25 and 0.5 equiv/mol. Therefore, it offers much more space per cation varying between 0.93 and 1.87 nm^2 (≈1.75 nm^2/cation in case of volclay).[25] That is, there is about 4 times as much space/cation on the volclay surface, which gives the chains more freedom to assume different conformations. Consequently, the molecular arrangement and phase present in alkylammonium SAMs on montmorillonite can be quite different.

The DSC traces (Figure 2) show relatively sharp peaks for 3C18 and 4C18, indicating reversible transitions with appreciable ΔH, whose nature can only be spectroscopically elicited. In contrast, 3C4, 4C4, 3C8, and 4C8, which have the same number of chains, did not show any abrupt change in enthalpy down to −30 °C, suggesting that the spatial distribution and packing density of the chains are not the only factors determining the phase present. The DSC trace of C18 that has the same chain length as 3C18 and 4C18 also did not show any peaks. That is, the combination of chain length and number of chains attached to the nitrogen atom (packing density) seems to be the origin of the transitions observed in DSC. The increase in entropy across the transition temperature in 2C18−4C18 indicates a loss in molecular order.

It is now well appreciated that FTIR spectroscopy is a sensitive tool for probing the molecular structure and dynamics of alkyl chains.[24,26−30] The wavenumber and intensity of the asymmetric ($\nu_{as}(CH_2)$) and symmetric ($\nu_s(CH_2)$) methylene stretching bands near 2920 and 2850 cm^{-1}, respectively, were found to be sensitive to changes in the gauche/trans conformer ratio and the lateral chain−chain interactions. For example, on melting nonadecane, i.e., on going from the crystalline phase (all-trans conformation) to a disordered liquid state rich in gauche population, $\nu_s(CH_2)$ and $\nu_{as}(CH_2)$ were shifted from 2848 to 2853 cm^{-1} and from 2916 to 2923 cm^{-1}, respectively.[22] These vibration modes were used to monitor changes in the conformation of alkyl chains assembled on different substrates with temperature.[26−36] The maxima of the corresponding absorption bands of alkylammonium SAMs on mica were also found to shift to higher frequencies at defined temperatures, indicating an order−disorder phase transition.[22,24] A similar shift to higher frequencies was observed in the $\nu_{as} + \nu_s$ CH_2 stretching bands of 2C18−4C18 on heating across the transition temperatures detected by DSC, indicating conformational changes in the alkyl chains (Figures 3 and 4). At ambient temperature, 3C18 showed an asymmetric stretching band at 2914 cm^{-1}, suggesting a high population of the trans conformer similar to that present in crystalline nonadecane. On heating, the absorption frequency increased to 2918.5 cm^{-1} between 43 and 50 °C (Figure 4). This increase parallels that of nonadecane on melting; however, the high-temperature absorption frequency is not as high as that of the isotropic liquid paraffin, indicating closer packing. The asymmetric stretching band of 4C18 experienced a similar shift (from 2915 to 2920 cm^{-1}) across the phase transition measured by DSC. On heating, the $\nu_s(CH_2)$ bands of 3C18 and 4C18 were also shifted from 2847.5 to 2850 cm^{-1} and from 2848.5 to 2851 cm^{-1}, respectively, indicating a change in conformation. The proximity of the low- and high-temperature absorption frequencies of these SAMs to those of crystalline and liquid nonadecane suggests that they undergo a similar order−disorder phase transition on heating. It may be remarked that the temperatures indicated by the DSC peak maxima correspond to those at which most of the frequency shifts were accomplished. However, the onset temperature in the DSC trace, whose accurate determination is known to be difficult, is ca. 30 °C lower. The asymmetric stretching band ($\nu_{as}(CH_2)$) of 2C18 also showed a frequency shift on heating; however, the shift temperature corresponded to the shoulder preceding the DSC peak and not to the peak temperature (Figure 2). At the moment, we have no explanation for the presence of a double peak in 2C18. None of the C4−4C4, C8−4C8, and C18 SAMs showed a frequency shift up to 70 °C and their absorption wavenumbers were around 2850 and 2920 cm^{-1}, construing disordered phases.

The results discussed above can be rationalized on the basis of increasing packing density and attraction forces between the alkyl chains with increasing length and number of chains attached to the nitrogen atom, leading to dominating trans conformation and ordered phases. On heating across the transition temperature, the gauche population increases and the tethered alkyl chains adopt a disordered (liquidlike) state with a random conformation. Taking into consideration that one end of the chain is fixed to the surface, it becomes clear that translational disorder is not possible and complete disorder as in an isotropic liquid cannot exist.

NMR spectroscopy has been used to probe the structure, conformation, and dynamics of alkyl chains, and the results obtained are not only complementary to FTIR but also give insight into the conformational heterogeneity and packing differences of the chains at interfaces.[24,37−40] In solid crystalline alkanes, the ^{13}C chemical shift of the methylene groups of ordered all-trans conformers is 33−35 ppm, whereas in solution dynamic averaging of all possible conformations (exchange averaged trans and gauche) leads to an average shift of 29−30 ppm. As in 2C18 mica, both all-trans and dynamic averaged gauche/trans conformations are observed in 2C18−4C18 volclay at ca. 33 and 30 ppm, respectively, depending on temperature, but the lines are generally broader (Figure 5). This is probably due to the influence of the available larger space/cation in volclay (mica 0.47 nm^2, volclay 1.75 nm^2) on the chain dynamics. The narrower resonances on mica imply higher order in 2C18 mica than in 4C18 volclay. Obviously, the larger space/cation on montmorillonite leads to lower packing density and allows more magnetic sites to be adopted by the alkyl chains. On going from 4C18 to C18, the available space/alkyl chain increases and the observed line width increases dramatically, as shown in the ^{13}C spectra at 65 °C (Figure 6) for the same reason.

At low temperatures, the methylene resonance position indicates a well-ordered all-trans conformation in 3C18 and 4C18 (Figure 7). With increasing temperature, the contribution from the dynamically disordered phase increases, leading to a gradual growth of the 30 ppm peak at the cost of the all-trans peak, indicating an order−disorder transition. This transforma-

tion extends over a temperature range and demonstrates the coexistence of ordered and disordered segments below and above the phase transition. The temperatures at which the 33 ppm peak become minimal compare well to the transition temperatures indicated by IR and DSC. The 1:1 all-trans to averaged gauche/trans ratio is reached at a temperature slightly higher than 35 °C in 3C18, that is, at a higher temperature than in 4C18 (26 °C), which is also in agreement with the DSC results. In 2C18, the dominance of the 33 ppm signal at low temperatures could not be observed down to −19 °C, indicating the presence of gauche segments even at such temperatures. Consequently, less order and looser packing than in 3C18 or 4C18 can be expected in 2C18. In contrast to 4C18 and 3C18, where the conformer ratio needed ca. 25 °C to change from 1:1 to a dominance of the averaged gauche/trans, 2C18 needed ca. 55 °C to achieve the same conversion. This is in line with the increasing widths of the DSC peaks on going from 4C18 to 2C18. The increase in averaged gauche/trans to all-trans ratio with temperature in 2C18−4C18 suggests an order−disorder transition, and the significantly sharper lines obtained for the averaged trans/gauche conformations indicate their higher mobility compared to those of the crystalline all-trans conformers.

The X-ray measurements show that the basal-plane spacing of volclay has been widened from ca. 1.2 nm (sodium form) to 1.4−3.5 nm by the cation exchange, depending on the number and length of the chains in the alkylammonium cation (Figure 10). It can also be seen that the C4−3C4 and C8 SAMs have the same thickness, viz., 0.46 nm (*d*-spacing, thickness of the aluminosilicate layer), which corresponds to the cross-sectional diameter of an alkyl chain rather than to the length of the chains in those cations (ca. 0.8−1.5 nm). The IR spectra of these SAMs did not show any temperature dependence, and the CH_2 absorption frequencies pointed to a disordered state. Their NMR spectra also showed resonances around 30 ppm for the methylene groups typical for a dynamic average between gauche and trans conformers. All these results indicate that the alkyl chains of these SAMs lie flat on the silicate surface in a disordered state, leading to a liquidlike phase. Because the alkyl chains are confined between two aluminosilicate layers attracted to each other by Coulombic forces with one end tethered to the substrate, i.e., they cannot be squeezed out, they are forced to fill the available space getting as close as possible.

The organic layer thickness increased slightly to 0.53 nm in 4C4 and a little more (0.65 nm) in 2C8, indicating that the volume of the organic matter became larger than that available between the silicate layers and that the alkyl chains started to force the layers to come apart. Neither the IR nor the NMR spectra of these SAMs indicated a conformation change, so that it can be assumed that the same phase continues to exist. On increasing the number of octyl chains from 1 to 4 (C8−4C8), the *d*-spacing increased linearly to match the increase in volume of the organic matter (Figure 10). The linearity of that increase as well as the DSC and spectroscopic results indicate that the molecules of these SAMs are similarly disordered as those of C4−4C4 and that no conformational transformation occurred.

C18 has a thickness of 0.88 nm (independent of temperature) intermediate between 2C8 (0.65 nm) and 3C8 (0.93 nm), corresponding to the total number of carbon atoms in the alkyl chains, and its IR and NMR spectra as well as DSC trace suggest a disordered state. In contrast, the thickness of 2C18 is temperature dependent (Figure 9) in accordance with the IR and NMR spectra, which suggests an ordered state at low temperatures and a conformational transformation of the chains

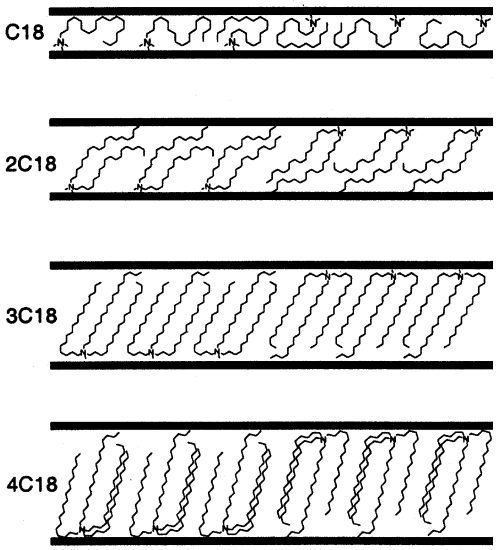

Figure 11. Schematic representation of possible structures of C18−4C18 SAMs on montmorillonite.

leading to a disordered state on heating. On the basis of the monolayer thickness at ambient temperature (1.44 nm), a bilayer arrangement (∼5 nm) of the molecules attached to silicate layers facing each other can be ruled out. Such an arrangement would require the molecular axis to be inclined to the surface normal by an angle larger than 70°, which is not consistent with the molecular geometry and the ordered state present. The alternatives are interdigitating chains radiating away from the surface at a tilt angle or a flat lying "pseudotrimolecular arrangement". However, it is hard to see how an ordered state can be achieved in a flat lying trimolecular layer and an interdigitating arrangement, in which the chains attend tilted upright positions, is more liable (Figure 11). A ca. 55° tilt angle of the average molecular axis to the surface normal would account for the layer thickness. The angle calculation is based on a molecular length of 2.6 nm.[41] Because the growth mechanism of C18 SAM on the mica surface was shown to start with islands (clusters), which grow and coalesce with progressing exchange, it can be expected that the molecules of 2C18 will build clusters on the montmorillonite surface.[42] This assumption is supported by the fact that the available area/cation on montmorillonite (1.75 nm^2) is much larger than that required by the 2C18 molecules; that is, the fully exchanged SAM in this case resembles the early stages of C18 on mica. Furthermore, the attractive forces between the alkyl chains favor the formation of clusters. To cope with all these facts, we suggest that the clusters of the dioctadecylammonium ions, attached to silicate layers facing each other, interdigitate to fill in the space (Figure 11).

The 3C18 and 4C18 SAMs had slightly differing thicknesses at RT (2.43 and 2.59 nm, respectively), which increased by 0.04 and 0.14 nm, respectively, on heating across the phase transition temperatures. These layer thicknesses suggest either a bilayer arrangement with an average molecular axis tilted by ca. 70° to the surface normal or an interdigitating arrangement of molecules slightly inclined to the surface normal. The geometry of these bulky molecules that have the shape of a garden claw (Figure 12) and the high degree of order spectroscopically observed support the second version. Because the surface area of the substrate is larger than that required by the organic molecules, we suggest an arrangement of interdigitating clusters, in which the average molecular axis is tilted by ca. 20° to the surface normal in 3C18 and is parallel to it in 4C18 (Figure 11). The increase in thickness across the phase transition

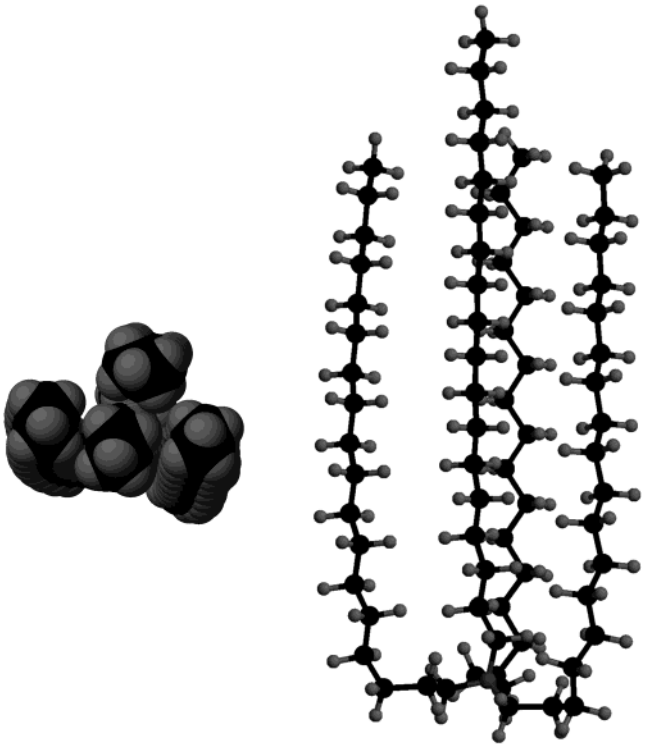

Figure 12. Side and top view of a molecular model of the tetraoctadecylammonium moiety with parallel alkyl chains (MM3 in CAChe WorkSystem Pro, Version 5.02, Fujitsu Ltd. 2002).

temperature in 2C18−4C18 can be attributed to the expected lower density of a disordered (liquidlike) phase compared to that of an ordered one, leading to an increase in volume. It may be remarked that the 3C18 SAM, whose molecules have a larger cross-sectional area than those of 2C18, has a smaller *d*-spacing on volclay (4.33 nm) than 2C18 on mica (4.77 nm), indicating different molecular arrangements on these two substrates. Therefore, an interdigitating arrangement on montmorillonite and a bilayer arrangement on muscovite were suggested.[24]

Conclusions

At ambient temperatures, alkylammonium monolayers assembled on montmorillonite adopt a two-dimensional order or a disordered state, depending on the cross-sectional area of the molecules, the area/cation available on the substrate, and the alkyl chain length. In the ordered state, the molecules attend an upright position with an average molecular axis inclined to the surface normal by an angle that depends on the molecular geometry and the packing environment. Molecular clusters attached to silicate layers facing each other interdigitate to fill the space available on the substrate surface. At low temperatures, the alkyl chains preferentially assume an all-trans conformation. Conformational transformation of the chains takes place with increasing temperature, leading to a disordered phase (liquidlike) in which the chains assume a random conformation. Translation disorder of the molecules in this dynamically disordered phase rich in gauche population is hindered by the electrostatic binding of the headgroups to the substrate. The transition from a dominant ordered trans conformation to a dynamically disordered state extends over a temperature range and manifests itself in IR-absorption frequency and carbon resonance shifts as well as in an increase in *d*-spacing and an entropy change. In contrast to alkylammonium SAMs on muscovite, the molecules do not adopt a bilayer arrangement on montmorillonite due to the larger area/cation available.

Acknowledgment. We thank Felix Bangerter for his performance on the NMR spectrometer. We also gratefully acknowledge financial support from the Swiss National Science Foundation (SNF).

References and Notes

(1) Bailey, S. W. *Reviews in Mineralogy*; Virginia Polytechnic Institute and State University: Blacksburg, 1984; Vol. 13.
(2) Brindley, G. W.; Brown, G. In *Crystal Structures of Clay Minerals and their X-ray Identification*; Brindley, G. W., Brown, G., Eds.; Mineralogical Society: London, 1980.
(3) Jasmund, K., Lagaly, G., Eds. *Tonminerale und Tone*; Steinkopff-Verlag: Darmstadt, 1993.
(4) Giannelis, E. P. *Appl. Organomet. Chem.* **1998**, *12*, 675.
(5) Theng, B. K. G. *The Chemistry of Clay-Organic Reactions*; Adam Hilger: London, 1974.
(6) Weiss, A. *Angew. Chem., Int. Ed. Engl.* **1963**, *2*, 134.
(7) Lagaly, G. *Solid State Ionics* **1986**, *22*, 43.
(8) Lagaly, G.; Benecke, K. *Colloid Polym. Sci.* **1991**, *269*, 1198.
(9) Lagaly, G. *CMS Workshop Lectures* **1994**, *6*, 1.
(10) Vaia, R. A.; Teukolsky, R. K.; Giannelis, E. P. *Chem. Mater.* **1994**, *6*, 1017.
(11) Newman, A. C. D.; Brown, G. In *Chemistry of Clays and Clay Minerals*; Newman, A. C. D., Ed.; Longman: Essex, 1987; p 59.
(12) Olis, A. C.; Malia, P. B.; Douglas, L. A. *Clay Miner.* **1990**, *25*, 39.
(13) Meier, L. P.; Kahr, G. *Clays Clay Miner.* **1999**, *47*, 386.
(14) Osman, M. A.; Suter, U. W. *J. Colloid Interface Sci.* **2000**, *224*, 112.
(15) Osman, M. A.; Ploetze, M.; Suter, U. W. *J. Mater. Chem.* **2003**, *13*, 2359.
(16) Bennett, A. E.; Rienstra, C. M.; Auger, M.; Lakshmi, K. V.; Griffin, R. G. *J. Chem. Phys.* **1995**, *103*, 6951.
(17) Campbell, G. C.; Crosby, R. C.; Haw, J. F. *J. Magn. Reson.* **1986**, *69*, 191.
(18) Haw, J. F.; Campbell, G. C.; Crosby, R. C. *Anal. Chem.* **1986**, *58*, 3172.
(19) Aliev, A. E.; Harris, K. D. M. *Magn. Reson. Chem.* **1994**, *32*, 366.
(20) Bielecki, A.; Burum, D. P. *J. Magn. Reson. A* **1995**, *116*, 215.
(21) Mildner, T.; Ernst, H.; Freude, D. *Solid State NMR* **1995**, *5*, 269.
(22) Osman, M. A.; Seyfang, G.; Suter, U. W. *J. Phys. Chem. B* **2000**, *104*, 4433.
(23) Osman, M. A.; Suter, U. W. *Chem. Mater.* **2002**, *14*, 4408.
(24) Osman, M. A.; Ernst, M.; Meier, B.; Suter, U. W. *J. Phys. Chem. B* **2002**, *106*, 653.
(25) Lagaly, G.; Schulz, O.; Zimehl, R. *Dispersionen und Emulsionen*; Steinkopff-Verlag: Darmstadt, 1997.
(26) Scheuing, D. R. *Fourier Transform Infrared Spectroscopy in Colloid and Interface Science*; ACS Symposium Series 447; American Chemical Society: Washington, DC, 1990.
(27) Dubois, L. H.; Nuzzo, R. G.; Allara, D. L. *J. Am. Chem. Soc.* **1990**, *112*, 558.
(28) Snyder, R. G.; Hsu, S. L.; Krimm, S. *Spectrochim. Acta, Part A* **1978**, *34*, 395.
(29) Snyder, R. G.; Strauss, H. L.; Elliger, C. A. *J. Phys. Chem.* **1982**, *86*, 5145.
(30) Bardeau, J. F.; Parikh, A. N.; Beers, J. D.; Swanson, B. I. *J. Chem. Phys.* **2000**, *104*, 627.
(31) MacPhail, R. A.; Strauss, H. L.; Snyder, R. G.; Elliger, C. A. *J. Phys. Chem.* **1982**, *88*, 334.
(32) Porter, M. D.; Bright, T. B.; Allara, D. L.; Chidsey, C. F. D. *J. Am. Chem. Soc.* **1987**, *109*, 3559.
(33) Nuzzo, R. G.; Korenic, E. M.; Dubois, L. H. *J. Chem. Phys.* **1990**, *93*, 767.
(34) Naselli, C.; Rabolt, J. F.; Swalen, J. D. *J. Chem. Phys.* **1985**, *82*, 2136.
(35) Nuzzo, R. G.; Dubois, L. H.; Allara, D. L. *J. Am. Chem. Soc.* **1990**, *112*, 558.
(36) Ulman, A. *Adv. Mater.* **1991**, *3*, 298.
(37) Badia, A.; Gao, W.; Singh, L.; Demers, L.; Cuccia, L.; Reven, L. *Langmuir* **1996**, *12*, 1262.
(38) Badia, A.; Singh, L.; Demers, L.; Cuccia, L.; Brown, G. R.; Lenox, R. B. *Chem. Eur. J.* **1996**, *2*, 359.
(39) Wang, L. Q.; Liu, J.; Exarhos, G. J.; Flangian, K. Y.; Bordia, R. *J. Phys. Chem. B* **2000**, *104*, 2810.
(40) Kubies, D.; Jérôme, R.; Grandjean, J. *Langmuir* **2002**, *18*, 6159.
(41) Okuyama, K.; Soboi, Y.; Iijima, N.; Hirabayashi, K. *Bull. Chem. Soc. Jpn* **1988**, *61*, 1485.
(42) Hayes, W. A.; Schwartz, D. K. *Langmuir* **1998**, *14*, 5913.